2026 IEEE International Conference on Robotics and Automation (ICRA 2026)
June 1-5, 2026. Vienna, Austria

Energy-Based Auto-Tuning of Velocity Flow Controller for Exoskeleton-User Speed Synchronization

Lyndon Tang[1], Bhavya Giri Goswami[2], Atusa Ghorbani Siavashani[2], John McPhee[2], Rezvan Nasiri[1], Arash Arami[1,3] *Member, IEEE*

***Abstract*— The Velocity Flow Field (VFF) lower-limb exoskeleton controller is widely applicable for gait rehabilitation because it provides the user with considerable agency over their gait; however, previous studies reported the feeling of "walking through water", and resistance to the user's efforts. In this work, a mathematical explanation for the viscous damping behaviour when users deviate from the reference trajectory, is presented. The controller was corrected and an adaptation law is proposed that synchronizes the speed gain with the user's current walking speed by minimizing the average mechanical work transferred between the user and the exoskeleton per step. Experiments comparing a fixed and adaptive controller with 12 participants walking at 0.4 ± 0.1 body length/s on a treadmill showed that the adaptive controller tracks changes in walking speed, while reducing the energy absorbed by $0.589 \pm 0.126 \frac{J}{\text{step}}$ compared to the fixed controller at the fastest walking speed. Analysis of changes in muscle effort and interaction torques with a human-exoskeleton interaction portrait showed that for most participants, the adaptive controller at medium and fast speeds substantially reduced user-controller disagreement and increased user agency over the walking motion. These positive results suggest that optimizing the energy supplied per step can serve as an effective coordination mechanism, enabling personalized and real-time adjustments of walking speed between the user and the exoskeleton.**

I. Introduction

Lower-limb robotic exoskeletons provide high-dose gait training and support daily activities for individuals with motor impairments, promoting motor learning and adaptation [1], [2]. They are particularly effective in individuals with residual voluntary motor function, such as after a stroke or incomplete spinal cord injury. Their success, however, relies on well-coordinated human–robot interaction, since active user engagement is essential to stimulate the neuromuscular system and drive recovery. To achieve this, various control strategies have been developed that range from intuitive assistance control to facilitate user adaptation, to advanced methods that minimize user-robot conflict, foster coordinated behaviours, or adapt assistance to the user's intended movement. Feedforward assistive controllers are a simple way to provide repeatable baseline assistance that supports the user in achieving the desired task. The actions of the exoskeleton can be triggered by gait cycle events, neuromuscular signals, or temporal synchronization signals [3]–[5]; however, they may fail to promote user engagement as they do not account for user's contribution to locomotion.

To promote user engagement and achieve natural synchronization, impedance-based control strategies allow the exoskeleton to intervene only when the user deviates considerably from a desired trajectory and otherwise remains passive, through virtual mechanical impedance, channels, and static force fields [3], [4]. This control approach is often referred to as the assist-as-needed paradigm. This is achieved through various techniques such as dead-zones [6], variable impedance control [7], optimal control within desired dynamical and kinematic constraints (i.e. control barrier functions) [8], and static force fields [9]. The effectiveness of these designs relies on the successful coordination between the intended movements of the user and the exoskeleton, which is negotiated through the sensory and actuation mechanisms of both agents. Coordination of the exoskeleton with the user requires the exoskeleton to alter its behaviour and adjust to the abilities and unique tendencies of the user.

The Velocity Flow Field (VFF) controller is an assist-as-needed controller that uses velocity fields in the hip-knee joint space that coerce the user towards and along a desired trajectory [9], [10]. Its simple but intuitive velocity-based control law has been shown to be more forgiving to error compared to energy-based path controllers and provides users with substantive agency over their gait [10]; however, studies have shown that poorly tuned parameters can lead to a decreased range of motion and viscous damping behaviour that feels like "walking through water" [11], which is confirmed in this study by showing that the control law resembles viscous damping under specific circumstances.

This study shows that the VFF control law can be decomposed into corrective and assistive components, resulting in two novel contributions: 1) an explanation and correction for the viscous damping effect that can suppress user's contribution, and 2) an auto-tuning method for a modified VFF controller that dynamically synchronizes assistance with the user's speed and effort across walking speeds.

This research was funded in part by NSERC Discovery grant number RGPIN-2024-06873, and in part by the New Frontiers in Research Fund-Exploration grant number NFRFE2022-620.

[1]Lyndon Tang, Rezvan Nasiri and Arash Arami are with the Department of Mechanical and Mechatronics Engineering, University of Waterloo, Waterloo, ON, N2L3G1, Canada le2tang@uwaterloo.ca; arash.arami@uwaterloo.ca

[2]Bhavya Giri Goswami, Atusa Ghorbani Siavashani, and John McPhee are with the Department of Systems Design Engineering, University of Waterloo, Waterloo, ON, N2L3G1, Canada b4goswam@uwaterloo.ca; a9ghorba@uwaterloo.ca; mcphee@uwaterloo.ca

[3]Arash Arami is also with KITE Institute, Toronto Rehabilitation Institute, University Health Network, Toronto, ON M5G2A2, Canada.

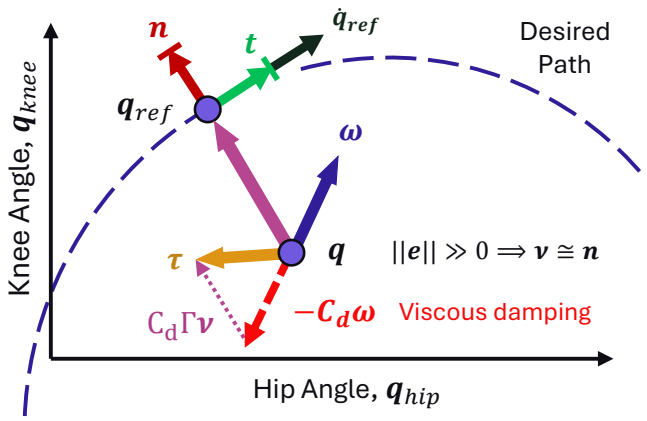

Fig. 1. The original control law torque (yellow) comprises a corrective (pink) and viscous damping term (red) when the current joint configuration is far from the desired path, in this case resisting knee flexion and hip extension of the swing leg.

II. Background

A. Analysis of the VFF Control Law

The VFF control law defines a time-invariant velocity field in the hip-knee joint space that flows towards a predefined reference path, corresponding to the typical hip and knee flexion trajectories during the swing phase of a gait cycle [9]. The flow control torque law in [9] is defined as

$$\boldsymbol{\tau} = C_d(\boldsymbol{\omega}_{ref} - \boldsymbol{\omega}) \tag{1}$$

where $\boldsymbol{\tau} \in \mathbb{R}^2$ is the vector of motor torques at the hip and knee joint, $C_d = 0.016\ \frac{Nms}{deg}$ is the gain of the control law described as analogous to the *drag coefficient* of the velocity field in [9], $\boldsymbol{\omega} = \dot{\boldsymbol{q}} \in \mathbb{R}^2$ is the vector of hip and knee flexion angular speeds. The *reference velocity*, $\boldsymbol{\omega}_{ref} = \Gamma\nu \in \mathbb{R}^2$, is a unit vector, $\boldsymbol{\nu} \in \mathcal{S}^1$, scaled by the *nominal path speed*, $\Gamma \in \mathbb{R}_+$.

$$\boldsymbol{\nu} = \frac{\|\mathbf{e}\|^2}{\sqrt{\|\mathbf{e}\|^4 + k_{sh}^2}}\mathbf{n} + \frac{k_{sh}}{\sqrt{\|\mathbf{e}\|^4 + k_{sh}^2}}\mathbf{t} \tag{2a}$$

$$= \sigma(\mathbf{e})\mathbf{n} + \bar{\sigma}(\mathbf{e})\mathbf{t} \tag{2b}$$

where $\mathbf{e} = \mathbf{q}_{ref} - \mathbf{q} \in \mathbb{R}^2$ is the *path error*, which is the vector between the current hip-knee joint configuration, $\mathbf{q} \in \mathbb{R}^2$, and the nearest joint configuration on the reference path, $\mathbf{q}_{ref} \in \mathbb{R}^2$, $\mathbf{n} \in \mathcal{S}^1$ is the unit vector in the direction of the error, and $\mathbf{t} \in \mathcal{S}^1$ is the unit vector tangent to the reference path at the nearest reference joint configuration, in the direction of motion during a typical gait cycle. The *shape parameter*, $k_{sh} = 16$ is defined in [9].

For notational convenience, the scaling factors, $\sigma(\mathbf{e}) \in [0, 1)$ and $\bar{\sigma}(\mathbf{e}) \in (0, 1]$ are defined such that $\|\boldsymbol{\nu}\| = \sqrt{\sigma^2(\mathbf{e}) + \bar{\sigma}^2(\mathbf{e})} = 1$. The normal and tangential components of the reference velocity are inversely coupled by this constraint so that when $\|\mathbf{e}\| \geq \sqrt{k_{sh}}$, with equality marking the crossover point, the normal (corrective) component starts dominating.

Substituting Eq.(2) into Eq.(1) and rearranging gives

$$\boldsymbol{\tau} = \underbrace{C_d\Gamma\sigma(\mathbf{e})\mathbf{n}}_{\boldsymbol{\tau}_c} + \underbrace{C_d(\Gamma\bar{\sigma}(\mathbf{e})\mathbf{t} - \boldsymbol{\omega})}_{\boldsymbol{\tau}_a} \tag{3}$$

The control law can be decomposed into two interpretable components. The *corrective torque*, $\boldsymbol{\tau}_c \in \mathbb{R}^2$, is entirely dependent on the path error, bounded in magnitude between $[0, C_d\Gamma)$, and redirects the user's joint configuration towards the reference path. The *assistive torque*, $\boldsymbol{\tau}_a \in \mathbb{R}^2$ regulates the joint velocity to flow tangent to the path. In extreme cases, large error causes $\boldsymbol{\nu} \simeq \mathbf{n}$, meaning that the control is dominated by corrective torques and the objective is to bring the user closer to the reference path. On the other hand, a small error causes the assistive torques to dominate ($\boldsymbol{\nu} = \mathbf{t}$), and the control objective is to regulate the current joint velocities to the *nominal path velocity*, $\dot{\mathbf{q}}_{ref} = \Gamma\mathbf{t} \in \mathbb{R}^2$, in the tangential direction.

A problem in the original control law, evident from the expression for $\boldsymbol{\tau}_a$, is that with large errors, $\boldsymbol{\tau}_a \simeq -C_d\boldsymbol{\omega}$ behaves like a viscous damper. Consequently, if the reference trajectory is poorly tuned for the user, the controller consistently resists the user's movements, producing a feeling of "walking through water".

B. User-Controller Agreement and Energy Transfer

The power supplied by the exoskeleton can be formulated by $P = \boldsymbol{\tau}^T\boldsymbol{\omega} \in \mathbb{R}$. If the motor torque and joint speed are of the same sign, the exoskeleton supplies power to the system; if they have opposite signs, it absorbs power from the system. Thus, the sign of power indicates whether the exoskeleton supports or opposes the motion. The work done by the exoskeleton (i.e., the total mechanical work exchanged), during each step, is the time integral of power:

$$E_{step} = \int_{T_{step}} (\boldsymbol{\tau}^T\boldsymbol{\omega})dt \tag{4}$$

and is one of the indicators of the overall user-exoskeleton coordination [12], [13]. If the exoskeleton is constantly absorbing energy from the user, then, on average, the mechanical work is negative, and the exoskeleton is opposing motion more than it encourages. In [11], large negative energy values caused crouch walking and shuffling. On the other hand, overly positive values were associated with a perception of jittery, unpredictable motion, and large pushes from the exoskeleton. Thus, ideally, the exoskeleton power contribution should not be negative or highly positive.

C. User-Controller Interaction Portraits

A recent study proposed a novel visual evaluation framework, called interaction portrait (IP), to qualitatively assess the effect of controllers on user–exoskeleton interaction [14]. IP represents the change in muscular effort and interaction torques between two controllers as a two-dimensional variable. An increase in both muscular effort and interaction torques (first quadrant, Q1) indicates greater disagreement, whereas a decrease in both (third quadrant, Q3) reflects a reduced disagreement. On the other hand, a decrease

in interaction torques with increased muscle effort (second quadrant, Q2) attributes to the user taking control over the exoskeleton, while an increase in interaction torques with decreased muscle effort (fourth quadrant, Q4) shows the user yields control to the exoskeleton.

III. METHODS

In this section, modifications to the original VFF controller, along with a novel adaptive algorithm that uses energy transfer to autonomously tune the nominal path speed (Γ) of the controller are shown. The experimental protocol conducted to compare fixed and adaptive versions of the controllers is then shown.

A. Modified VFF Control Law

Three modifications were made to the assistive component of the original control law in Eq.(3).

First, given the separate roles of the corrective and assistive torques and the different roles that Γ plays in each component, distinct parameters Γ_c and Γ_a were assigned for the corrective and assistive components, respectively. In accordance with the assist-as-needed paradigm, $\Gamma_c = 266\ ^\circ/s$ was set to a constant value, corresponding to the average path speed observed from a representative participant walking at medium speed ($0.4\ BL/s$), which is the proposed value in [11], to assert that the desired kinematic pattern is always pursued.

In the assistive torques, Γ_a is the desired speed along the reference path under ideal zero-error conditions; thus, the parameter was augmented to vary along the path so that the reference joint velocities match the kinematic trajectories during normal, unassisted walking, which indeed vary significantly over the gait cycle [11]. The nominal path velocity was replaced with $\dot{\mathbf{q}}_{ref}(\theta) : [0, 1) \to \mathbb{R}^2$, a fixed, parametric function of the normalized step time, $\theta \in [0, 1)$, fit to the typical joint velocities during unassisted walking at $0.4\ BL/s$ with least squares regression. A scaling factor, $\gamma_a \in \mathbb{R}_+$, then modulates the nominal joint velocities to control the desired gait speed. This is equivalently interpreted as using a phase-varying $\Gamma_a = \gamma_a \|\dot{\mathbf{q}}_{ref}(\theta)\|$ since the tangent direction can be expressed as $\mathbf{t} = \frac{\dot{\mathbf{q}}_{ref}}{\|\dot{\mathbf{q}}_{ref}\|}$ [11].

The next modification aimed to resolve the viscous damping behaviour that emerges when the path error is large as shown in Fig.1. The user's current joint velocity, $\boldsymbol{\omega}$ was decomposed into normal and tangential components, $\boldsymbol{\omega}_n = \text{proj}_n(\boldsymbol{\omega})$, $\boldsymbol{\omega}_t = \text{proj}_t(\omega) \in \mathbb{R}^2$. The damping behavior was mitigated by gating the tangential component of the user's current angular velocity by $\bar{\sigma}(\mathbf{e})$. Consequently, in high error cases, no damping occurs along the path due to the $-C_d\boldsymbol{\omega}_t$ term, and in low error cases, the speed along the path is regulated so that $\boldsymbol{\omega}$ converges to $\gamma_a\dot{\mathbf{q}}_{ref}$. For notational convenience, let $\boldsymbol{\omega}_{\bar{\sigma}} = \boldsymbol{\omega}_n + \bar{\sigma}(\mathbf{e})\boldsymbol{\omega}_t \in \mathbb{R}^2$ be the *tangentially gated joint velocities*. The normal component was not modified to avoid any unwanted oscillations around the reference trajectory and preserve the stability behaviour of the original controller.

Lastly, the estimated Coriolis and gravitational torques of the exoskeleton (derived through the Euler-Lagrange equation), $H_e = \hat{h}_e(\mathbf{q}, \dot{\mathbf{q}})$, were added to compensate for its inertia. Thus, the modified controller was given by:

$$\boldsymbol{\tau} = \underbrace{C_d\left[\Gamma_c\sigma(\mathbf{e})\mathbf{n} - \boldsymbol{\omega}_n\right]}_{\boldsymbol{\tau}_c} + \underbrace{C_d\bar{\sigma}(\mathbf{e})\left[\gamma_a\dot{\mathbf{q}}_{ref} - \boldsymbol{\omega}_t\right]}_{\boldsymbol{\tau}_a} + H_e \quad (5)$$

Note that the terms *corrective* and *assistive* are only used to distinguish the components of the exoskeleton torques, but both of them contribute to supporting the user.

B. Adaptive Nominal Path Speed Tuning

When the path error is small, which is asserted by the corrective torques, then $\bar{\sigma}(\mathbf{e}) \simeq 1$, and the sign of the assistive torque in Eq.(5) depends on the signs of the hip and knee elements of $\gamma_a\dot{\mathbf{q}}_{ref} - \boldsymbol{\omega}$. Consequentially, assistance is applied and power is supplied if the reference velocity is higher than the user's, whereas resistance is given and power is absorbed if the reference velocity is lower than the user's. This principle is used to automatically select the minimal level of assistance through an autonomous adaptation law that selects γ_a. Notably, only assistive energy is optimized to prevent resistance or over-assistance, while the corrective action is preserved.

The power transferred by the exoskeleton is,

$$P = \left[C_d\Gamma_c\sigma(\mathbf{e})\mathbf{n} + C_d(\gamma_a\bar{\sigma}(\mathbf{e})\dot{\mathbf{q}}_{ref} - \boldsymbol{\omega}_{\bar{\sigma}})\right]^T\boldsymbol{\omega} \quad (6)$$

The distributive property of the dot product allows us to decompose the power into the corrective and assistive components.

$$P_c = C_d\Gamma_c\sigma(\mathbf{e})\mathbf{n}^T\boldsymbol{\omega} \quad (7a)$$

$$P_a = C_d\gamma_a\bar{\sigma}(\mathbf{e})\dot{\mathbf{q}}_{ref}^T\boldsymbol{\omega} - C_d\boldsymbol{\omega}_{\bar{\sigma}}^T\boldsymbol{\omega} \quad (7b)$$

The power supplied by the exoskeleton due to the assistive torque is affine with respect to γ_a; thus, the energy supplied by the exoskeleton is as well.

$$E_a = \gamma_a\int_{T_{step}}\left[C_d\bar{\sigma}(\mathbf{e})\dot{\mathbf{q}}_{ref}^T\boldsymbol{\omega}\right]dt - \int_{T_{step}}\left[C_d\boldsymbol{\omega}_{\bar{\sigma}}^T\boldsymbol{\omega}\right]dt \quad (8)$$

For notational simplicity, the scale and bias terms in Eq.(8) are defined as

$$a = \int_{T_{step}}\left[C_d\bar{\sigma}(\mathbf{e})\dot{\mathbf{q}}_{ref}^T\boldsymbol{\omega}\right]dt \quad (9a)$$

$$b = -\int_{T_{step}}\left[C_d\boldsymbol{\omega}_{\bar{\sigma}}^T\boldsymbol{\omega}\right]dt \quad (9b)$$

The adaptation objective is to choose γ_a so that the assistive work done by the exoskeleton is regulated to a desired setpoint, E^*. This is equivalent to minimizing the cost function $J(\gamma_a) = \frac{1}{2}(a\gamma_a + b - E^*)^2$ while keeping γ_a positive and bounded below a predefined limit ($\bar{\gamma}_a$) to avoid excessive, uncomfortable torques on the user. The corresponding problem is:

$$\begin{aligned}\arg\min_{\gamma_a} \quad & \frac{1}{2}(a\gamma_a + b - E^*)^2 \\ \text{s.t.} \quad & 0 \le \gamma_a \le \bar{\gamma}_a\end{aligned} \quad (10)$$

Since the experiments involved able-bodied participants, we set $E^* = 0$, providing no tangential assistance to alter joint speeds. For users with motor deficits, however, a positive E^* should be used increasing with the desired assistance level. Moreover, since E_a depends on the user's energy contribution to the system, through changes in the joint velocities, and the user's behavior is widely varying across individuals and time-varying based on the user's intent, the objective function is quasi-static. An online Accelerated Projected Gradient Descent (APGD) was used to continually solve the constrained optimization problem for γ_a [15], [16]. In Algorithm-1, the projection operator, $S : \mathbb{R} \rightarrow \mathbb{R}$ is

Algorithm 1 Accelerated Projected Gradient Descent Step

Input: $\gamma_a[k], E^*, k \geq 0$
Output: $\gamma_a[k+1]$

function UPDATE STEP($\gamma_a[k]$)
  $\hat{a}[k] \leftarrow \int_{T_k}(C_d\bar{\sigma}(\mathbf{e})\dot{\mathbf{q}}_{ref}^T\boldsymbol{\omega})dt$
  $\hat{b}[k] \leftarrow -\int_{T_k}(C_d\boldsymbol{\omega}_\sigma^T\boldsymbol{\omega})dt$
  $\delta[k] \leftarrow \frac{k-2}{k+1}$
  $y[k+1] \leftarrow \gamma_a[k] + \delta[k](\gamma_a[k] - \gamma_a[k-1])$
  $\nabla_{\gamma_a}J(y[k+1]) \leftarrow \hat{a}[k](\hat{a}[k]y[k+1] + \hat{b}[k] - E^*)$
  $\gamma_a[k+1] \leftarrow \mathrm{S}(\gamma_a[k] - \beta\nabla_{\gamma_a}J(y[k+1]))$
  return $\gamma_a[k+1]$
end function

the saturation operation, and $\delta, \beta \in \mathbb{R}_+$ are the momentum factor and the learning rate, respectively. The learning rate was $\beta = 0.05$ and the update frequency of γ_a was $0.5\ Hz$ to allow the user to feel the change in torques and make adjustments for the next step.

C. Experimental Protocol and Evaluation

The proposed auto-tuning method was evaluated by comparing a controller with an adaptive value of γ_a (*adaptive controller*) to a version with a fixed $\gamma_a = 1$ (*fixed controller*) on an Indego Explorer exoskeleton (Ekso Bionics, USA), at slow, medium, and fast walking speeds on an instrumented treadmill (Bertec, USA), corresponding to 0.3, 0.4, and 0.5 body lengths per second. For the adaptive controller, a separate value of γ_a was optimized for each leg.

Twelve participants (6 male, 6 female, age: $26 \pm 4\ years$, body mass: $69.5 \pm 21.3\ kg$, height: $1.71 \pm 0.06\ m$) with no known neuromuscular impairment participated in the study. The participants provided informed consent prior to the experiment. The study protocol was conducted in accordance with the Declaration of Helsinki and approved by the Research Ethics Board, ORE#41794.

The session (Fig.2B) consisted of two sections, one with the fixed controller and one with the adaptive controller, presented in randomized and blinded order. Each section started with a $30\ s$ calibration period at $0.4\ BL/s$, during which the exoskeleton inertial dynamics were compensated but no VFF controller was applied. Participant's average hip and knee flexion angle and velocity trajectories over the last

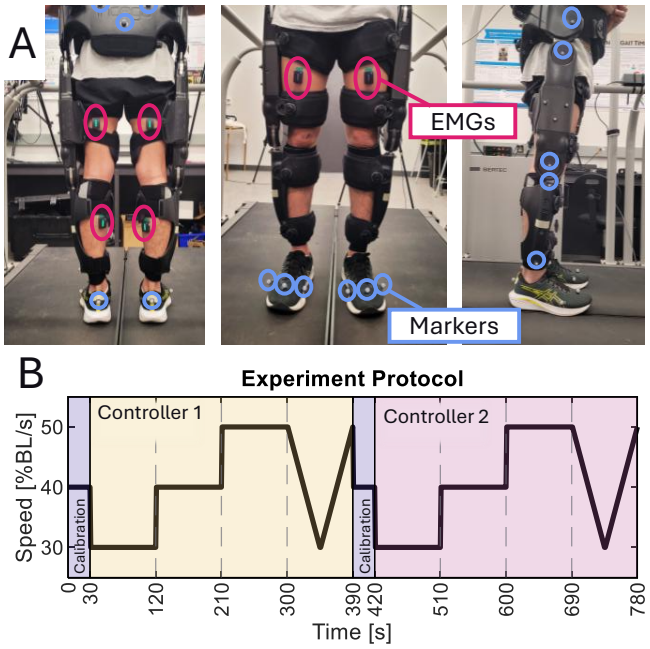

Fig. 2. A) Muscle activities are measured with surface electromyography sensors (pink), while kinematics are measured with retroreflective Vicon motion capture markers (blue) and exoskeleton joint encoders. B) Experiment protocol is composed of two sections, one for each fixed and adaptive controllers (randomized order).

twenty seconds, were recorded for the reference path. After calibration, participants completed three steady-state walking conditions at 0.3, 0.4, 0.5 BL/s for 90 s each, followed by a 45 s linear speed ramp down from $0.5 - 0.3\ BL/s$, and back, termed the dynamic condition. Across participants, the mean slow, medium, and fast treadmill speeds were $0.514 \pm 0.019\ m/s, 0.685 \pm 0.026\ m/s, 0.856 \pm 0.032\ m/s$. After each condition, participants rated their perceived disagreement feeling with the controller relative to the passive exoskeleton in calibration as a baseline, and at the end, they indicated their preferred controller (first or second).

The embedded joint encoder sensors in the exoskeleton were used to measure joint angles and velocities at a sampling rate of 200 Hz. Retro-reflective motion capture markers (Vicon, UK) were used on the heel, as well as the first, third, and fifth metatarsal (MP) joints of each foot to record the kinematics of the feet downsampled from 2000 Hz to 200 Hz as shown in Fig.2A. Muscle activities were measured with surface electromyography (EMG) sensors (Trigno, Delsys, USA) placed on the Rectus Femoris (RF), long head of the Biceps Femoris (BF), and medial head of the Gastrocnemius (GM) at a sampling frequency of 2000 Hz. EMG signals were bandpass filtered to $10 - 450\ Hz$ with a fourth-order Butterworth filter, followed by full-wave rectification and smoothing with a fourth-order $8\ Hz$ Butterworth filter. The EMG data was then downsampled to 200 Hz before normalization to the maximum EMG value observed throughout the whole trial for each participant. Human-exoskeleton interaction torques at each joint were estimated with the neural network method used in [14] that converts

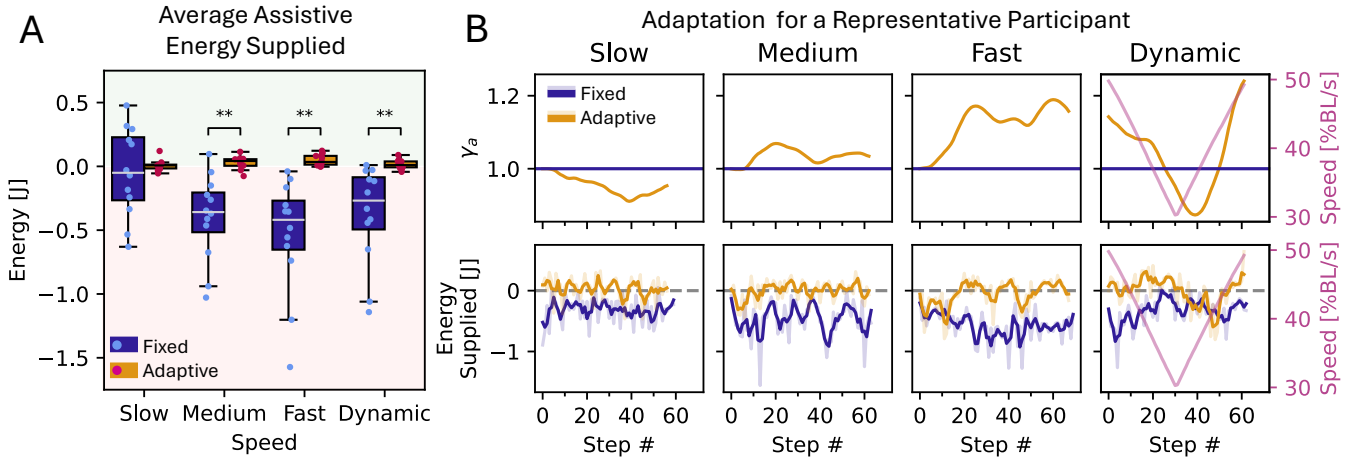

Fig. 3. A) Average energy supplied by assistive torques per step across all participants. B) Value of the nominal path speed scaling factor (top) adapts to changes in the walking speed for a representative participant, causing the energy supplied per step by assistive torques (bottom) to stay close to zero even though the speed changes. The three-step average is overlaid on the instantaneous energy per step (faded).

time-delayed measurements of joint kinematics to interaction torques.

To build the IP, muscle effort, which is the integral of squared muscle activities over every step, was calculated as a physiological cross-sectional area (PCSA)-based weighted averaged of RF, BF, and GM muscles. The PCSA-based weights (RF: 13.5 cm^2, BF: 10.8 cm^2, GM: 21.0 cm^2) are proportional to their maximum muscle force value [14], [17]. The normalized interaction torques were computed by taking the integral of the absolute value of the estimated interaction torques of the hip and knee joints, normalized by the maximum amplitude in each trial. Both the values for the adaptive controller were centered and scaled around the average values from the fixed controller and plotted with the difference in torque magnitudes along the x-axis, and the difference in muscle effort along the y-axis.

The average root mean squared path error (RMSE) and *path speed* ($\|\dot{\mathbf{q}}(\theta)\|_2$), joint ranges of motion, and power trajectories were computed for the participant's dominant leg. Spatiotemporal gait metrics, including the maximum height of the foot during the swing phase (peak foot clearance), step duration, and stride length, were computed from the foot marker trajectories. In steady-state conditions, statistics were computed from the final $45s$ of each condition.

A Friedman test with a significance level of $\alpha = 0.05$ was used to evaluate group-level differences in average statistics for each participant between the fixed and adaptive controllers. A post-hoc Wilcoxon signed-rank test with $\alpha = 0.05$ and Bonferroni correction was then used to analyze the differences at each speed.

IV. Results

In this section, the performance of the adaptive controller is compared with the fixed controller based on assistive energy transferred by the exoskeleton, spatiotemporal gait metrics, as well as the user's behavior through IP analysis and average muscle activation. Numerical results are presented as median ± inter-quartile range (IQR).

A. Energy and Power Transfer

The Friedman test comparing energy supplied by the assistive torques showed statistically significant differences between the fixed and adaptive controllers ($p \ll 0.001$). The Wilcoxon Signed Rank test further confirmed that, at medium, fast, and dynamic speeds, the energy supplied by assistive torques was significantly higher (all $p \leq 0.001$) for the adaptive controller compared to the fixed version see Fig.3A. There was no significant difference between the controllers at slow speed ($p = 0.677$).

The energy absorbed by the fixed controller per step increased from an average of -0.050 ± 0.494 $\frac{J}{\text{step}}$ at slow speeds to -0.358 ± 0.311 $\frac{J}{\text{step}}$ at medium speeds, -0.419 ± 0.384 $\frac{J}{\text{step}}$ at fast speeds and -0.268 ± 0.409 $\frac{J}{\text{step}}$ during the dynamic condition. In contrast, the average energy transferred by adaptive assistive torques per step was much smaller in magnitude with lower variance with 0.00756 ± 0.02982 $\frac{J}{\text{step}}$, 0.0419 ± 0.0517 $\frac{J}{\text{step}}$, 0.0347 ± 0.0688 $\frac{J}{\text{step}}$, and 0.0108 ± 0.0464 $\frac{J}{\text{step}}$ for slow, medium, fast, and dynamic speeds, respectively, as shown in Fig.3A.

The mean power transferred at each joint for a representative participant, shown in Fig.4, clarifies when the exoskeleton assists or resists motion during the gait cycle. At the hip, the fixed controller had negative peaks at mid-stance (70 % of gait cycle) as extreme as -0.652 ± 0.994 W at slow speeds, while those peaks were positive for the adaptive controller, up to 1.50 ± 0.92 W at fast speeds. At the knee, the fixed controller had two negative peaks up to -1.84 ± 1.39 W (fast) at the beginning and end of the swing phase ($60, 90$ % of gait cycle), which were reduced in amplitude to 0.567 ± 0.490 W (medium) for the adaptive controller.

The top row of Fig.3B shows the adaptation of γ_a as the walking speed changes for a representative participant. For

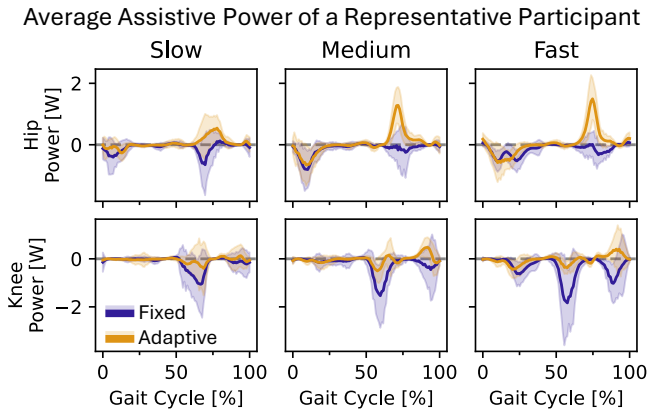

Fig. 4. The mean trajectory with unit standard deviation confidence intervals of power supplied to the hip (top) and knee (bottom) joints by the assistive torques for a representative participant.

each of the steady-state speeds, the initial reference velocity starts with a scale of 1, and changes to keep the energy supplied per step (bottom row) close to zero. In slow speed, the scaling factor reduces to a minimum of 0.910 and a final value of 0.954, while in medium speed, the scaling factor peaked at 1.07 and ended at 1.03, and for fast speed, peaked at 1.19 and ended at 1.16. In the dynamic condition, the scaling factor γ_a starts its final value from the fast walking (1.09). As the treadmill speed drops, the assistive energy of the adaptive controller is positive, indicating that the exoskeleton is supplying surplus energy, causing γ_a to drop. Once the treadmill ramps up again, so does γ_a (following a delay of 8 steps).

B. Controller Regulation Objectives

The adaptive controller showed no significant changes in corrective behaviour, compared to the fixed controller, as expected since the two controllers share the same corrective control component. The Friedman test comparing both controllers at the group level showed no significant differences in the RMSE ($p = 0.175$), peak foot clearance ($p = 0.773$), hip and knee range of motions ($p = 0.273$, $p = 0.525$), step duration ($p = 0.954$), and the stride length ($p = 0.977$).

Fig.5A shows that across all participants, the average RMSE per step is reasonable. The median RMSE is at worst $6.08 \pm 0.38°$ and $5.49 \pm 0.38°$ during the fast walking condition for fixed and adaptive controllers, respectively.

The spatiotemporal gait metrics measured in this experiment align with reported values in the literature [18]. During dynamic walking across all speeds, the average peak foot clearance was 21.6 ± 1.4 cm with the fixed controller and 22.2 ± 1.9 cm with the adaptive controller (Fig.5B). Hip and knee ranges of motion were $39.2 \pm 3.6°$ and $43.9 \pm 14.2°$ for the fixed controller, compared to $39.7 \pm 4.1°$ and $45.6 \pm 13.2°$ for the adaptive controller. Step duration decreased from 1.57 ± 0.13 s and 1.58 ± 0.14 s at slow speed to 1.27 ± 0.12 s and 1.30 ± 0.13 s at fast speed, for the fixed and adaptive controllers, respectively. Stride length ranged from 0.786 ± 0.120 m (slow) to 1.06 ± 0.16 m (fast) with the fixed

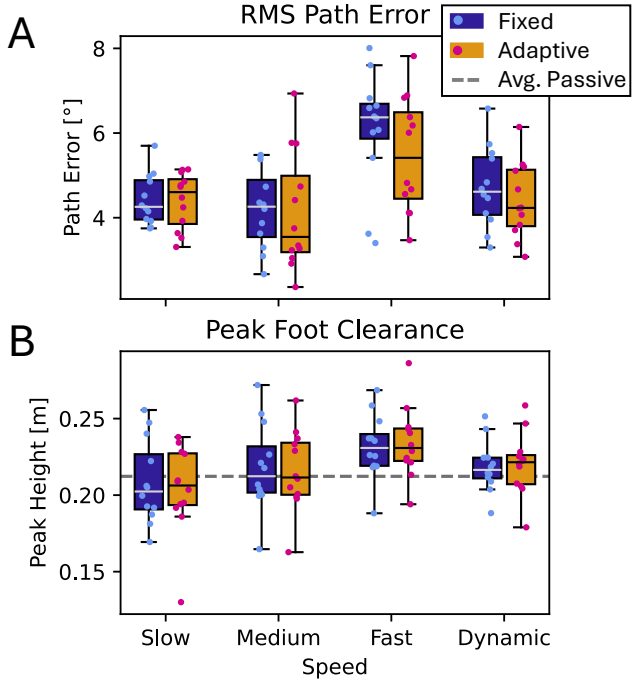

Fig. 5. A) Participant average path tracking error. B) Average peak height of the foot above the ground.

controller, and from 0.790 ± 0.098 m (slow) to 1.07 ± 0.12 m (fast) with the adaptive controller.

C. Interaction Portrait and Muscle Activation

The IP plot in Fig.6A compares the average muscular effort and interaction torques for all participants during the last $20s$ of the adaptive controller with those of the fixed controller. At slow speeds, users either took control over the exoskeleton (four users in Q2) or yielded control (five in Q4). At medium speeds, eight participants had decreased interaction torques (Q2/3), while at fast speeds seven participants had reduced muscle effort (Q3/4).

The progression of user-exoskeleton interaction over time for one of participants with respect to the average interaction observed for the fixed controller is shown in Fig.6B. For all three speeds, the adaptive interaction trends towards Q2 and Q3, corresponding to decreased interaction torques. At fast walking, while adaptive controller result in reduced disagreement (points fall in the Q3), the fixed controller led to increased disagreement.

Fig.7 compares the difference in the PCSA-weighted average muscle activation across participants. Positive values indicate increased muscle activation with the adaptive controller, while negative values reflect decreases relative to the average activation with the fixed controller. Although the Friedman test did not reveal a significant effect ($p = 0.341$), more than 75% of participants exhibited lower average muscle activation level during walking with the adaptive controller in medium, fast, and dynamic speeds. At the fast and dynamic speeds, some participants experienced reductions in muscle activation up to 5%.

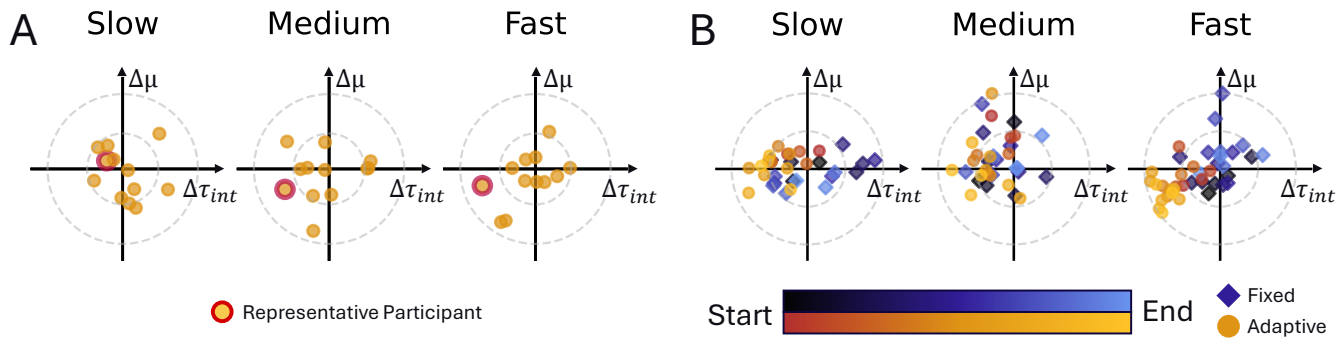

Fig. 6. A) Average difference in interaction between the last 20 s of the adaptive controller with respect to the last 20 s of the fixed controller for each participant. B) Temporal progression IPs of the representative participant highlighted in A, comparing every 4 steps of each controller with respect to the mean interaction value of the fixed controller over all points. Brighter points correspond to later steps.

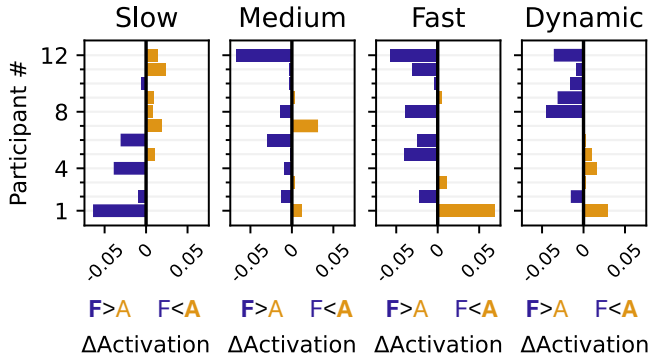

Fig. 7. Difference in the average muscle activation between the adaptive and fixed controllers for each participant.

V. Discussion

A. Modifications to the Original Flow Controller

The viscous damping behavior for large error scenarios in the original control law, explained in Fig.1, leads to power dissipation and fast fatigue where the average assistive energy in Fig.3A was typically negative for the fixed controller at the medium and fast speeds, requiring the user to exert more effort. This is arguably justifiable when the user cannot establish a safe gait pattern on their own, so the desired behavior is to halt user error and prioritize correction before continuing the motion. However, this damping behavior can also become obstructive when the desired path is not well tuned to the user's anthropometry, motor capacity or walking speed, which may be highly variable across users [19], [20].

Obstruction is particularly evident when the knee flexion angle of the swing leg is substantially lower than the desired value given the hip flexion angle, the scenario in Fig.1. The large path error causes the controller to act like a viscous damper along the direction of step progression. The resulting resistance, applied while the user is in an unstable position, inhibits further knee flexion and hip extension. This reduces the knee range of motion and foot clearance, increasing the risk of stumbling or falling, and worsens tracking error, thereby reinforcing undesired behavior.

The proposed control law, Eq.(5), does not inhibit user motion, even if the error is markedly large. In Eq.(5), $e \rightarrow 0 \Rightarrow \tau_a \rightarrow 0$, leaving only the corrective torques in the normal direction and no resistance in the tangential direction, allowing the user to converge more smoothly towards the desired path, thus it is only reasonable to compare the adaptive version of Eq.(5) to a fixed version, since the original controller, Eq.(1), will have more negative work than the fixed controller in Fig.3A.

In the dynamic condition, γ_a tracks the changes in treadmill speed (Fig.3B) demonstrating that the adaptive controller correctly reduces assistance when over-assisting at a slower speed and synchronizes with the user as they exert more energy to speed up.

The learning rate, β, and the update frequency in Algorithm (1) were chosen in the pilot experiments. Update frequencies above $0.7\ Hz$, or learning rates $\beta > 0.1$ caused large step-to-step fluctuations in γ_a, producing oscillatory changes in both the exoskeleton and user behaviour. Since the iterative APGD solver requires a consistent optimization problem across iterations, user behaviour must remain quasi-static, necessitating slow adaptation. The oscillations in γ_a in the last 20 steps of the steady-state conditions in Fig.3B show the user co-adapts to the changes in the joint torques from step-to-step. This suggests that the main limitation of faster adaptation rates is the user's ability to interpret, anticipate, and react to changes in exoskeleton behaviour.

For users with ambulatory deficits, the assistive energy setpoint, E^*, in Eq.(10), should be set to a positive constant to provide continual assistance. The encouraging results in this study suggest that the assistive energy is controllable to reach and hold an arbitrary setpoint.

B. User-exoskeleton Interaction and Feedback

Both the participant average and representative IPs in Fig.6 show that the adaptive controller outperforms the fixed version at all speeds by reducing the interaction torques while allowing the user to exercise agency without disagreement. Furthermore, in Fig.6B, the shift of points toward Q3 across all speed conditions indicates that the adaptive controller

progressively increased user-controller agreement over time.

In the questionnaire, 8 out of 12 participants preferred the adaptive controller and reported experiencing less resistance when walking, particularly at medium and fast speeds. Those who favored the fixed controller felt that the adaptive controller moved them along a different kinematic path than what they wanted. Also, they liked the stronger sense of assistance at slow speeds with the fixed controller, which emerges since the fixed controller was tuned for medium speed, causing positive assistive energy for slow speed, as shown in Fig.3A. This difference in preference is reflected in muscle activity in Fig.7, where certain participants had substantial decreases in muscle activity at all speeds, while others had increases.

C. Limitations and Future Work

Future work includes evaluating the controller in overground environments since overground walking leads to more frequent and varied changes in speed and intent in due to the environment.These dynamics challenge the quasi-static assumption underlying the optimization in Eq.(10).

Lastly, the VFF controller assumes a consistent kinematic reference path across speeds; however, joint trajectories vary with walking speed [19], [20]. In the VFF control law, large errors lead to corrective behaviour dominating assistive torques, limiting adaptation, and increasing user-exoskeleton disagreement. Participants who preferred the fixed controller may have had desired trajectories different from those at the (medium) calibration speed, causing unnecessary corrective torques. Further improvements should incorporate both velocity and trajectory adaptation, e.g., using [21].

VI. Conclusion

The adaptive and modified VFF controller resolves the damping behaviour in the original controller and reduces the disagreement between the user and the exoskeleton by modulating the desired joint velocities according to the sign of mechanical work. In an experimental study with 12 participants walking on a treadmill at $0.4 \pm 0.1\ BL/s$, the adaptive controller significantly reduced energy dissipation by the exoskeleton compared to the fixed controller while preserving corrective behavior and kinematics. Analysis of muscular effort and interaction torques using interaction portraits revealed that participants co-adapted well to the adaptive controller, showing less disagreement with the device and more frequently leading the motion, particularly at higher speeds, making it a preferred controller for majority. Nonetheless, four participants preferred the steady and predictable behavior of the fixed controller, specifically for slow speed. Overall, these encouraging results suggest that optimizing energy transfer between the user and the exoskeleton can improve walking speed synchronization by personalizing the reference path speed to each individual.

References

[1] M. Lotze, C. Braun, N. Birbaumer, S. Anders, and L. G. Cohen, "Motor learning elicited by voluntary drive," *Brain: A Journal of Neurology*, vol. 126, pp. 866–872, 2003.

[2] J. L. Emken, R. Benitez, and D. J. Reinkensmeyer, "Human-robot cooperative movement training: Learning a novel sensory motor transformation during walking with robotic assistance-as-needed," *Journal of NeuroEngineering and Rehabilitation*, vol. 4, no. 8, 2007.

[3] L. Marchal-Crespo and D. J. Reinkensmeyer, "Review of control strategies for robotic movement training after neurologic injury," *Journal of NeuroEngineering and Rehabilitation*, vol. 6, no. 20, 2009.

[4] R. Baud, A. R. Manzoori, A. Ijspeert, and M. Bouri, "Review of control strategies for lower-limb exoskeletons to assist gait," *Journal of NeuroEngineering and Rehabilitation*, vol. 18, no. 119, 2021.

[5] H. Dinovitzer, M. Shushtari, and A. Arami, "Feedforward control of lower limb exoskeletons: which torque profile should we use?" *IEEE Robotics and Automation Letters*, 2023.

[6] A. Duschau-Wicke, J. von Zitzewitz, A. Caprez, L. Lunenburger, and R. Riener, "Path control: A method for patient-cooperative robot-aided gait rehabilitation," *IEEE Transactions on Neural Systems and Rehabilitation Engineering*, vol. 18, no. 1, pp. 38–48, 2010.

[7] J. Lopes, C. Pinheiro, J. Figueiredo, L. P. Reis, and C. P. Santos, "Assist-as-needed impedance control strategy for a wearable ankle robotic orthosis," in *2020 IEEE International Conference on Autonomous Robot Systems and Competitions (ICARSC)*, 2020, pp. 10–15.

[8] T. Gurriet, M. Tucker, A. Duburcq, G. Boeris, and A. D. Ames, "Towards variable assistance for lower body exoskeletons," *IEEE Robotics and Automation Letters*, vol. 5, no. 1, pp. 266–273, 2020.

[9] A. Martínez, B. Lawson, and M. Goldfarb, "A controller for guiding leg movement during overground walking with a lower limb exoskeleton," *IEEE Transactions on Robotics*, vol. 34, no. 1, pp. 183–193, 2018.

[10] A. Martínez, B. Lawson, C. Durrough, and M. Goldfarb, "A velocity-field-based controller for assisting leg movement during walking with a bilateral hip and knee lower limb exoskeleton," *IEEE Transactions on Robotics*, vol. 35, no. 2, pp. 307–316, 2019.

[11] R. Nasiri, L. Tang, M. Goldfarb, and A. Arami, "Role of speed regulation and speed modulation in velocity-field based control," 2025, bioRxive preprint:676406.

[12] M. Sharifi, J. K. Mehr, V. K. Mushahwar, and M. Tavakoli, "Autonomous locomotion trajectory shaping and nonlinear control for lower limb exoskeletons," *IEEE/ASME Transactions on Mechatronics*, vol. 27, no. 2, pp. 645–655, 2022.

[13] N. Garcia-Hernandez, C. Munguia-Angeles, and V. Parra-Vega, "Assist-as-needed robotic strategy based on velocity fields for enhancing motor training," *IEEE/ASME Transactions on Mechatronics*, vol. 30, no. 2, pp. 1504–1513, 2025.

[14] M. Shushtari, J. Foellmer, and A. Arami, "Human–exoskeleton interaction portrait," *Journal of NeuroEngineering and Rehabilitation*, vol. 21, p. 152, 2024. [Online]. Available: https://jneuroengrehab.biomedcentral.com/articles/10.1186/s12984-024-01447-1

[15] R. Tibshirani, "Proximal gradient descent and acceleration," May 2015. [Online]. Available: https://stat.cmu.edu/~ryantibs/convexopt-S15/lectures/08-prox-grad.pdf

[16] S. Tan and J. Lu, "A nesterov's accelerated projected gradient method for monotone variational inequalities," 2022. [Online]. Available: https://arxiv.org/abs/2212.08346

[17] R. L. Lieber, T. J. Roberts, S. S. Blemker, S. S. M. Lee, and W. Herzog, "Skeletal muscle mechanics, energetics and plasticity," *Journal of NeuroEngineering and Rehabilitation*, vol. 14, no. 1, p. 108, 2017. [Online]. Available: https://jneuroengrehab.biomedcentral.com/articles/10.1186/s12984-017-0318-y

[18] C. A. Fukuchi, R. K. Fukuchi, and M. Duarte, "A public dataset of overground and treadmill walking kinematcis and kinetics in healthy individuals," *PeerJ*, vol. 6, p. e4640, 2018.

[19] ——, "Effects of walking speed on gait biomechanics in healthy participants: a systematic review and meta-analysis," *Systematic Reviews*, vol. 8, no. 153, 2019.

[20] J. Padulo, S. Rampichini, M. Borrelli, D. M. Buono, C. Doria, and F. Esposito, "Gait variability at different walking speeds," *Journal of Functional Morphology and Kinesiology*, p. 158, 2023.

[21] M. Shushtari, R. Nasiri, and A. Arami, "Online reference trajectory adaptation: A personalized control strategy for lower limb exoskeletons," *IEEE Robotics and Automation Letters*, vol. 7, p. 128–134, 2021.